NANO · MICRO small
www.small-journal.com

Enhancement of Single-Photon Purity and Coherence of III-Nitride Quantum Dot with Polarization-Controlled Quasi-Resonant Excitation

*Seongmoon Jun, Minho Choi, Baul Kim, Martina Morassi, Maria Tchernycheva, Hyun Gyu Song, Hwan-Seop Yeo, Noëlle Gogneau, and Yong-Hoon Cho**

III-Nitride semiconductor-based quantum dots (QDs) play an essential role in solid-state quantum light sources because of their potential for room-temperature operation. However, undesired background emission from the surroundings deteriorates single-photon purity. Moreover, spectral diffusion causes inhomogeneous broadening and limits the applications of QDs in quantum photonic technologies. To overcome these obstacles, it is demonstrated that directly pumping carriers to the excited state of the QD reduces the number of carriers generated in the vicinities. The polarization-controlled quasi-resonant excitation is applied to InGaN QDs embedded in GaN nanowire. To analyze the different excitation mechanisms, polarization-resolved absorptions are investigated under the above-barrier bandgap, below-barrier bandgap, and quasi-resonant excitation conditions. By employing polarization-controlled quasi-resonant excitation, the linewidth is reduced from 353 to 272 μeV, and the second-order correlation value is improved from 0.470 to 0.231. Therefore, a greater single-photon purity can be obtained at higher temperatures due to decreased linewidth and background emission.

1. Introduction

A quantum light source is an essential element for quantum photonic technologies, such as quantum sensing,[1,2] quantum computing,[3,4] and quantum communication.[5,6] Various systems including trapped atoms,[7] point defects,[8–11] and colloidal quantum dots (QDs),[12,13] have been studied to develop ideal quantum light source. However, epitaxially grown semiconductor QDs have received considerable attention because of their fast radiative recombination rate,[14] robustness, and scalability of on-chip integration with photonic[15–17] and electronic devices.[18–20]

Epitaxially grown QDs based on III-nitride material systems are among the most promising quantum emitters because of their deterministically polarized emission property[21] as well as their potential for high-temperature operation[22,23] due to their large exciton binding energy. Despite these advantages, two challenges remain for this material system. The first obstacle is the spectral diffusion[24,25] generated by the quantum-confined Stark effect. An exciton with an intrinsically large permanent dipole moment inside III-nitride QDs interacts with the fluctuating electric field caused by the trapping and detrapping of charge carriers in the vicinity, which results in the ambiguity of the exciton ground state energy. This phenomenon produces inhomogeneous linewidth broadening of the QDs and affects the coherence properties of III-nitride QD-based quantum light sources.

The second obstacle is background emission from undesired emitters that are formed in the neighborhood of the QDs. For Stranski–Krastanov QDs, the wetting layer and other QDs can act as unwanted emitters.[26–28] Moreover, emission from the quantum well, which is formed in the side facets of photonic structures, causes background emission in site-controlled QD cases[29–31] (e.g., QDs embedded in nanowires or pyramids). The background signal harms the single-photon purity and limits the performance of quantum information applications.

Several efforts have been made to overcome these problems by applying resonant excitation to the QD ground state. However, the resonant excitation scheme requires a separation of the excitation laser from the QD emission. Therefore, complex photonic systems such as waveguide-coupled QDs[32–34] or in-plane excitation laser[35,36] are necessary. In addition, blocking the excitation laser with a cross-polarization setup[37,38] is indispensable for achieving resonant excitation. However, the use of this polarization setup inevitably sacrifices the emission intensity of QDs.

S. Jun, M. Choi, B. Kim, H. G. Song,[+] H.-S. Yeo, Y.-H. Cho
Department of Physics and KI for the NanoCentury
Korea Advanced Institute of Science and Technology (KAIST)
291 Daehak-ro, Yuseong-gu, Daejeon 34141, Republic of Korea
E-mail: yhc@kaist.ac.kr

M. Morassi, M. Tchernycheva, N. Gogneau
Center for Nanosciences and Nanotechnologies
Paris-Saclay University
CNRS, UMR9001, Boulevard Thomas Gobert, Palaiseau 91120, France

The ORCID identification number(s) for the author(s) of this article can be found under https://doi.org/10.1002/smll.202205229.

[+]Present address: Sensor system research center, Korea Institute of Science and Technology (KIST), 5 Hwarang-ro 14-gil Seongbuk-gu, Seoul 02792, Republic of Korea

DOI: 10.1002/smll.202205229

Therefore, the quasi-resonant excitation (QRE) method, wherein the wavelength of the excitation laser resonates with the excited state of the QDs, such as the p-shell state or upper state, can be an alternative solution. QRE generates carriers in the excited state of the QDs directly, thereby suppressing both inhomogeneous linewidth broadening and unwanted background emission. In addition, the QD emission can be isolated from the laser owing to the different wavelengths. Previous research had employed the QRE to AlGaN/GaN QDs[39] and GaN/InGaN QDs.[40] However, these researches implemented the QRE only for coherent manipulation of the exciton state of a single QD. Therefore, adopting QRE to reduce linewidth broadening and background emission has not yet been achieved in III-nitride QD systems.

In this work, we conducted polarization-controlled QRE to InGaN QDs embedded in GaN nanowires to enhance the single-photon purity and coherence of single QD. In particular, we introduced polarization-controllability in QRE, which can selectively pump the intended excited state of the QD by excluding the contribution of continuum absorption levels caused by the crossed transitions. InGaN QDs in GaN nanowires were grown using plasma-assisted molecular beam epitaxy and dispersed on a silicon nitride wafer. We observed emission at 3.15 eV and the excited state of the QD at 3.206 eV by performing micro-photoluminescence (μ-PL) and μ-PL excitation (μ-PLE) experiments. To confirm the influence of the QRE on the QD, we compared its emission under three excitation wavelengths: 3.542, 3.303, and 3.206 eV, which correspond to the above-barrier bandgap excitation (ABE), below-barrier bandgap excitation (BBE), and QRE conditions, respectively. We measured the polarization-resolved absorption under the three excitation wavelengths and found contrasting excitation polarization properties arising from the different excitation mechanisms. By measuring with a higher-order grating, the linewidth broadening under polarization-controlled QRE became 78% of that in the ABE case. Moreover, the second-order correlation value under polarization-controlled QRE became 49.1% of that in the ABE case, due to the reduced background emission. Finally, the $g^{(2)}(0)$ value remained below 0.5, even at 100 K. In conclusion, we compared QD emission while changing the excitation wavelengths and polarizations and confirmed that the selection of excitation polarization is crucial in a QRE scheme. We expect that the polarization-controlled QRE technique, without sacrificing the measured intensity, could provide improvements to diverse platforms that suffer from unwanted background emission and a lack of coherence.

2. Results and Discussion

Figure 1a shows the ABE and QRE schemes. In ABE, the carriers generated at the GaN barrier by pumping laser undergo relaxation from the barrier states to the ground state of the QD. During this process, the fluctuation of the local electric field produced by the capture and de-capture events of carriers results in the spectral diffusion effect. However, in QRE schemes, direct pumping of electrons and holes to the excited states of the QD prevents spectral diffusion. To investigate the effect of QRE on the optical properties of QD quantum emitters, we used InGaN QDs embedded in the GaN nanowires. Figure 1b shows scanning electron microscopy (SEM) and transmission electron microscopy (TEM) images of the GaN nanowires. Thin InGaN QDs are located at the end of the nanowire. The average thickness and diameter of the QDs were obtained by TEM images

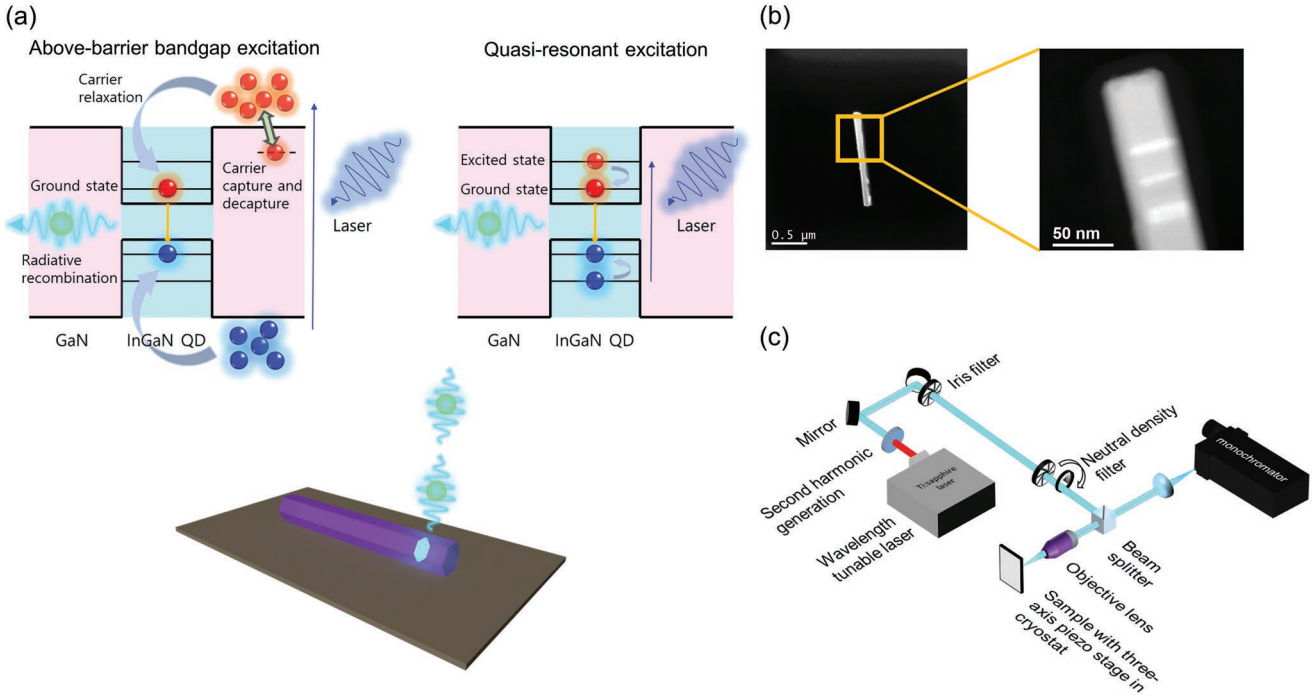

Figure 1. a) Schematic of the ABE and QRE processes. b) SEM and TEM images of the InGaN QD in a GaN nanowire dispersed on silicon nitride on a silicon wafer. c) Schematic of the μ-PL and μ-PLE experiment setup for a single QD.

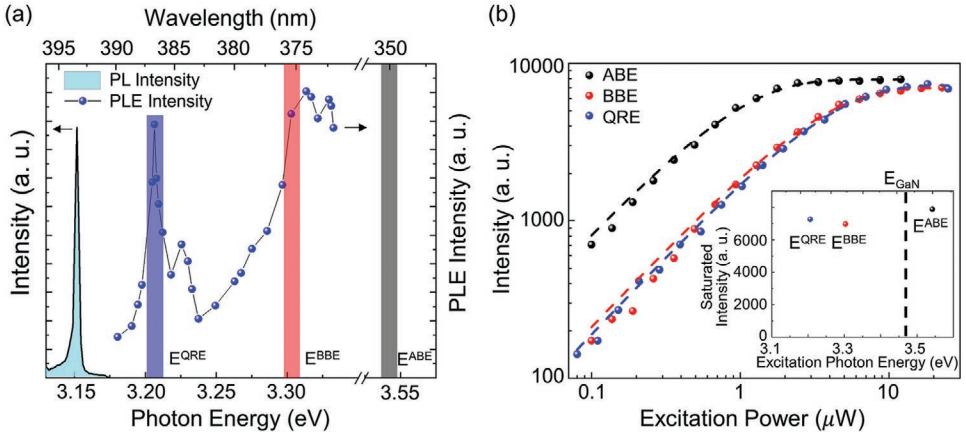

Figure 2. a) μ-PL and μ-PLE spectra of single InGaN QD measured at 10 K; shaded areas indicate the excitation wavelengths used in our experiments. b) Power-dependent PL intensity of a single QD excited by ABE, BBE, and QRE. The dashed lines represent the fitted results for investigating the QD saturation behavior. The inset shows the saturated intensities of the QD excited by ABE, BBE, and QRE.

of 30 QDs, which were 4.7 ± 0.3 and 38.9 ± 1.5 nm, respectively (Figure S5, Supporting Information). Since the GaN nanowires were grown on Si(111) substrate, the nanowire axis is the c-axis. The nanowires were dispersed on silicon nitride on a silicon wafer using the drop-casting method. Subsequently, 50 nm of Al_2O_3 was deposited via atomic layer deposition. To probe the excited state of a single QD, we performed μ-PL and μ-PLE spectroscopy under low-temperature conditions, as shown in Figure 1c. The QD intensity was measured while changing the wavelength of the excitation laser. The detailed experimental setup is explained in the methods section.

Figure 2a shows the μ-PL and μ-PLE results. The peak at 3.15 eV in the QD spectrum represents the ground state transition. The QD intensity decreased continuously with decreasing excitation photon energy until 3.25 eV. The PLE spectrum had a local maximum intensity at excitation of 3.206 eV, which was 55 meV above the ground state. Because the longitudinal optical (LO) phonon energy of GaN is 90 meV and that of InN is 72 meV, it is deduced that the 55 meV difference does not originate from the LO-phonon induced transition. In addition, the 55 meV difference is similar to the value in previous report on c-plane InGaN QDs.[41] Therefore, we attributed the peak in the PLE spectrum to the transition from the excited state to the ground state. The origin of the nonzero continuum absorption signal was assigned as alloy fluctuations of Indium and "crossed-transition". Crossed-transition means that the electron is generated at the barrier and the hole is generated at the discrete states of the QD, or vice versa.[42] To compare QRE with other excitations, we analyzed the emission for three types of excitation wavelength of the laser, which are indicated in the shaded area of Figure 2a. The E^{ABE} = 3.542 eV pumping laser excites the GaN barrier (whose bandgap is ≈3.47 eV at low temperature). However, the E^{BBE} = 3.303 eV laser does not excite the GaN barrier. In particular, the E^{QRE} = 3.206 eV laser resonates with the local maximum of the PLE spectrum. Figure 2b shows the excitation-power-dependent measurements of the QD intensity under three different excitation conditions. In each excitation condition, polarization selections in both excitation and emission path were used. In general, the emission of a single QD follows saturation behavior in the high-power regime, and the saturated intensity of the QD is not determined by the absorption efficiency of the excitation laser but the quantum efficiency of the QD. Thus, the saturated intensity remains unchanged under various excitation wavelength conditions if the same transition of the QD is observed. We fitted the power-dependent emission intensity using the following function:[43]

$$I = I_{\infty}\left(1 - e^{-\frac{P}{P_{sat}}}\right) \quad (1)$$

where I is the intensity of the QD, P_{sat} is the saturation power of the pumping laser, I_{∞} is the saturated intensity of the QD, and P is the pumping power. The saturated peak intensities of the QD with ABE, BBE, and QRE were 7882 ± 67, 6978 ± 52, and 7261 ± 72, respectively. Although the intensity of the QD was saturated at different powers under each excitation condition, the results showed that the saturated intensities under different excitation wavelength conditions were almost the same. It is worth noting that the same saturated intensities in QRE indicate that we did not need to sacrifice the QD intensity. The lower saturation power at ABE indicates that it generated more carriers than the other excitation conditions due to the pumping of the barrier states.

To analyze the mechanisms of the various excitation methods, we investigated the polarization-dependent absorption properties at different excitation wavelengths. As shown in **Figure 3**a, we obtained polarization-resolved μ-PL emission using a half-wave plate and linear polarizer in the emission path. Subsequently, the intensity of the QD emission was measured depending on the polarization angle of the excitation laser while fixing the polarization of the emission path. In Figure 3b, the emission of the QD shows linear polarization under the BBE laser with a linear polarization of 30°. The direction of linear polarization of our nanowire-embedded QD was perpendicular to the nanowire axis (Figure S1, Supporting Information). This is due to recombination between the ground state electron and a hole from the A-band, similar to the wurtzite structure InAs/InP QDs.[44] Figure 3c shows the polarization-resolved absorption in the ABE case. The polarization-resolved

absorption is nearly unpolarized and indicates the absence of polarization selectivity of the absorption due to the excitation of the GaN barrier. Figure 3d shows a schematic and the result of polarization-resolved absorption under BBE. As mentioned above, the continuum absorption of BBE originated from alloy fluctuations and crossed-transition.[42] Based on the geometry of the nanowire QD, the dipole direction of the crossed-transition follows the direction of the nanowire, as shown in the schematic in Figure 3d. However, the dipole direction originated from the alloy fluctuation might be random. Therefore, the polarization direction of the absorption which is parallel to the nanowire axis indicates that the dominant origin of continuum absorption is crossed-transition. This result is similar to that of a previous report on in-plane polarized absorption from crossed transition in a QD in-a-well system.[45] In contrast, the polarization direction of the absorption under QRE, which is parallel to the emission polarization, is orthogonal to the nanowire axis, as shown in Figure 3e.

To compare linewidth broadening under different excitation conditions, we measured the PL spectra of a single QD using a higher-order grating (3600 grooves per mm). In addition, to investigate the influence of excitation polarization, we used additional polarization selection in excitation, i.e., the maximum and minimum points in Figure 3d,e under BBE and QRE conditions. In the ABE, polarization selection on excitation was not used because it has an almost unpolarized excitation property. **Figure 4**a–c shows the PL spectra under ABE, BBE-pol. max. (polarization maximum point in Figure 3d), and QRE-pol. max. (polarization maximum point in Figure 3e), respectively. For appropriate comparison, the excitation pumping powers were manipulated to set a similar QD intensity for each condition. The linewidths of the QD under each excitation condition were fitted using the Voigt function. In Figure 4d, they have linewidths of 353 ± 2.49, 305 ± 3.76, 295 ± 2.69, 272 ± 1.98, and 295 ± 4.14 μeV under ABE, BBE-pol. max., BBE-pol. min. (polarization minimum point in Figure 3d), QRE-pol. max., and QRE-pol. min. (polarization minimum point in Figure 3e), respectively. As the ABE pumping laser generated numerous carriers in the barrier states, it had the broadest linewidth among the various excitation conditions owing to the large spectral diffusion. Although the BBE pumping laser excited the continuum states of the QD, it did not excite the barrier states. Consequently, the charge fluctuation could be reduced compared to that in the ABE case.

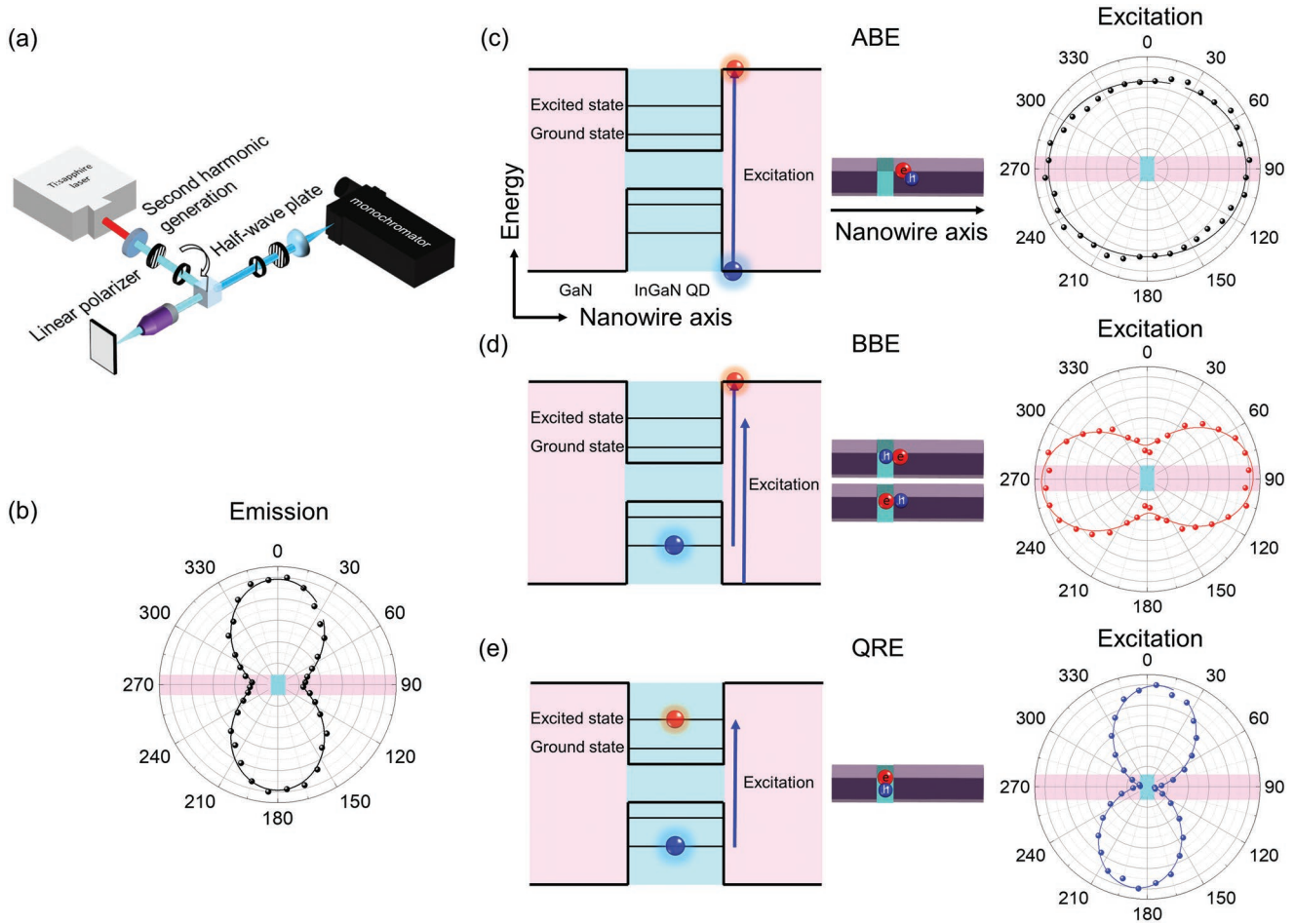

Figure 3. a) Schematic of experimental setup for polarization-dependent emission and excitation measurements. b) Polarization-dependent emission intensity of QD under BBE. Schematic and polarization-dependent excitation measurement under c) ABE, d) BBE, and e) QRE. The wire images (pink colors) in polarization-resolved emission and excitation results indicate the directions of the dispersed nanowire on a substrate.

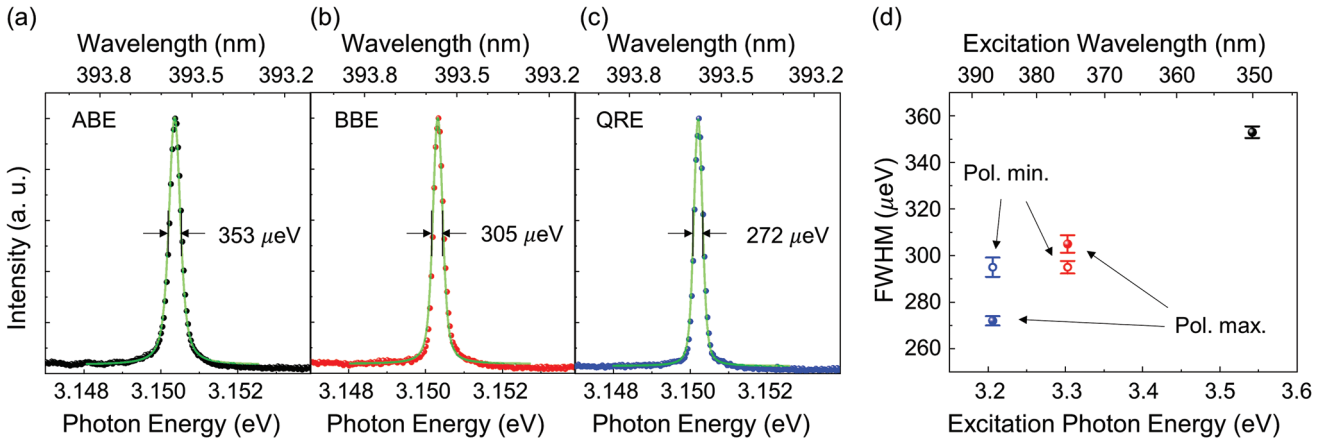

Figure 4. μ-PL spectra of a single QD excited by a) ABE, b) BBE, and c) QRE with a higher-order grating. In each excitation, the polarization of the laser was chosen to make the QD intensity maximum. The linewidth was fitted with a Voigt function. d) Linewidth of the single QD under different excitation wavelength conditions. The circle and hole symbols signify that the polarization of the laser matched with the maximum and minimum points of Figure 3, respectively.

In particular, the direct excitation of the QD excited state by means of QRE with proper polarization control can exclude the contribution attributed to the absorption of the continuum state, suppressing the spectral diffusion effect and reducing the linewidth broadening. Another piece of evidence of suppressed spectral diffusion under polarization-controlled QRE is the contraction of time-dependent peak wavelength fluctuation (Figures S3 and S4, Supporting Information). Although linewidth broadening was not sufficiently suppressed to achieve transform-limited single photon emission because the lifetime is 0.81 ns (Figure S2, Supporting Information) (transform-limited linewidth is ≈0.80 μeV), polarization-controlled QRE was effective in reducing linewidth broadening. Another remarkable point of the normalized spectra of the QD under various excitation conditions was the reduction in background emissions under QRE compared to that of the other excitation cases. The suppression of the background emission affects the attainment of high single-photon purity.

To confirm the improvement in single-photon purity under QRE, we measured the second-order autocorrelation using a Hanbury–Brown and Twiss experimental setup. **Figure 5**a shows the second-order correlation functions of the QD emission for each excitation condition. In the second-order correlation measurements, the emission intensities of the QD under each excitation condition were similar. To calculate the $g^{(2)}(0)$ value, we obtained the integrated coincidence counts of each peak and divided the integrated counts of zero delay by the average integrated counts of 10 peaks, which are five peaks on both sides of zero delay. The error was calculated using the standard deviation of the integrated counts of the ten peaks. Although the integrated counts at zero time delay are equal to zero for the ideal single-photon emitter, a nonzero value of $g^{(2)}(0)$ can be obtained due to background emission. In general, an emitter is regarded as a single-photon emitter when $g^{(2)}(0)$ is lower than 0.5. The values of $g^{(2)}(0)$ under each excitation condition were 0.470 ± 0.017, 0.385 ± 0.020, and 0.231 ± 0.010 for excitation of ABE, BBE-pol. max., and QRE-pol. max., respectively. Although the antibunching signal emerged under ABE, the $g^{(2)}(0)$ value was close to 0.5. However, $g^{(2)}(0)$ decreased to 0.385 under BBE-pol. max., which was probably induced by the decline of the background signal. Importantly, a dramatic change in the $g^{(2)}(0)$ value (0.231) was observed under QRE-pol. max.. To analyze the effects of the background signal on autocorrelation, we considered the theoretical relationship between the background signal and $g^{(2)}(0)$. The value of $g^{(2)}(0)$ due to the background level is expressed by the following equation:

$$g^{(2)}(0) = 1 - \left(\frac{S}{S+B}\right)^2 \quad (2)$$

where S and B are the signal and background intensity, respectively. In Figure 5b, we represent the measured $g^{(2)}(0)$ value with the corresponding S/(S + B) of the QD emission for the five excitation conditions, which are ABE, BBE-pol. max., BBE-pol. min., QRE-pol. max., and QRE-pol. min.. The green line indicates the ideal case, which follows the equation. As can be observed, the measured $g^{(2)}(0)$ values under the five different conditions were well suited to the ideal case. Therefore, we can confirm that the change in $g^{(2)}(0)$ originates from the degradation of background emission. Furthermore, by comparing the $g^{(2)}(0)$ values under QRE-pol. max. and QRE-pol. min., it is worth noting that polarization selection of the excitation laser is necessary to achieve high single-photon purity. The increase of single-photon purity is unclear in BBE since the degree of polarization of BBE absorption is small, as can be seen in Figure 3d. However, single-photon purity is improved apparent by additional polarization selection in the QRE scheme. On the one hand, III-nitride QDs are attractive platforms for room-temperature-operating quantum emitters due to their large exciton binding energy. However, the peak intensity of the QD decreased owing to linewidth broadening caused by phonon interactions at elevated temperatures. Consequently, the relatively increased background emission near the QD induced a reduction in the single-photon purity at elevated temperatures. Hence, the suppression of background emission is necessary to accomplish high-temperature operation of single-photon emitters. To investigate the influence of the suppressed background emission on single-photon purity under QRE at

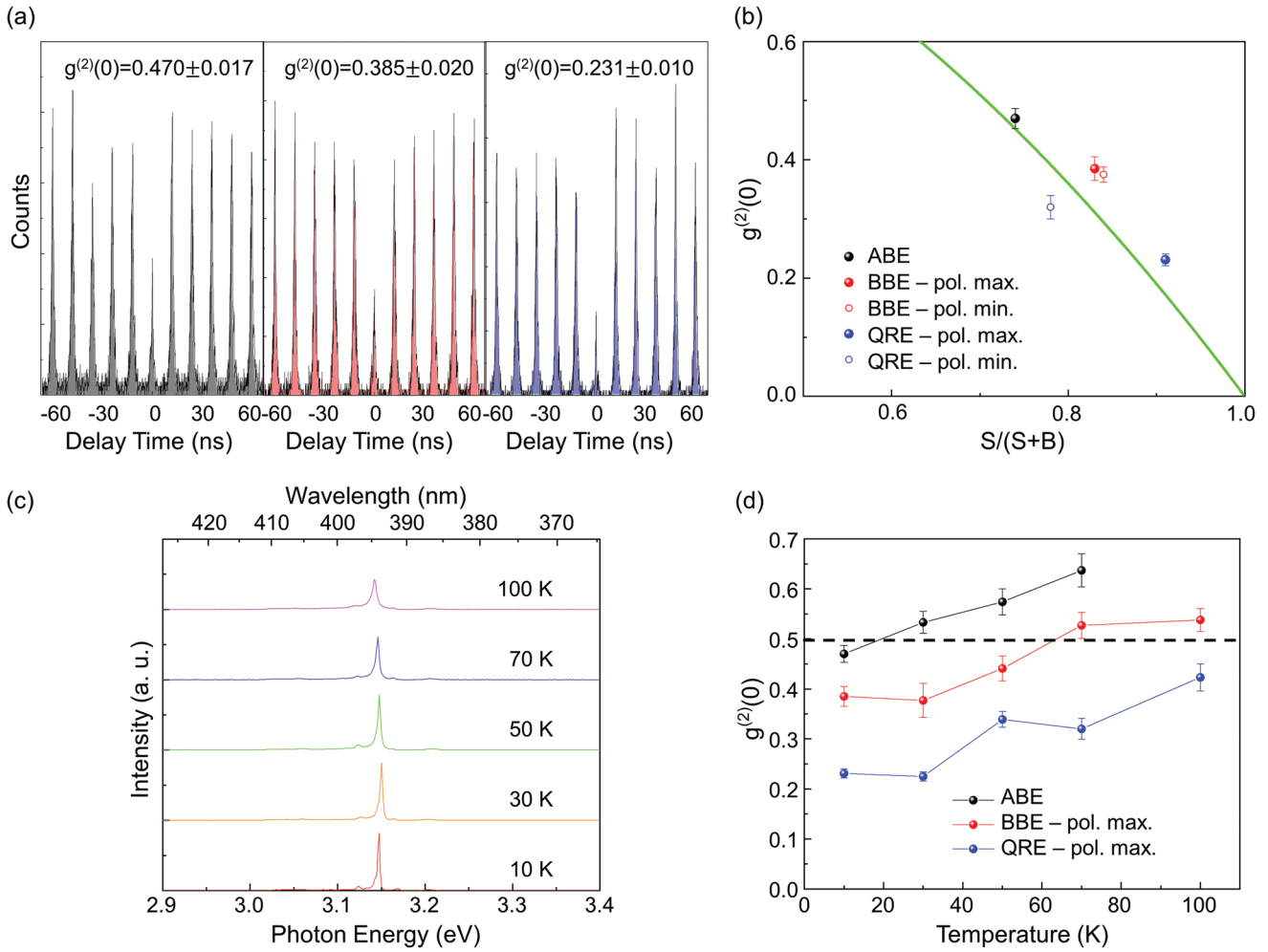

Figure 5. Second-order correlation function with pulsed laser under different excitation conditions using a) ABE (left), BBE-pol. max. (middle), and QRE-pol. max. (right). b) S/(S+B) of emission and corresponding measured $g^{(2)}(0)$ value under different excitation conditions. Green line is the theoretical relation between $g^{(2)}(0)$ and S/(S+B). c) Temperature-dependent μ-PL emission under QRE-pol. max. d) Temperature-dependent second-order correlation values under excitation of ABE (black), BBE-pol. max. (red), and QRE-pol. max. (blue).

elevated temperatures, we obtained temperature-dependent PL emission and second-order correlation under three excitation conditions: ABE, BBE-pol. max., and QRE-pol. max.. Figure 5c shows the temperature-dependent QD emission under polarization-controlled QRE. The QD emission showed redshift and linewidth broadening with increasing temperature. The redshift of the emission was caused by a change in the bandgap and linewidth broadening originated from interaction with phonons. In addition, a decrease in peak intensity was observed with increase in temperature. Figure 5d shows the temperature-dependent second-order correlations under excitation at ABE, BBE-pol. max., and QRE-pol. max.. When the temperature was increased, the second-order correlation value increased at each excitation wavelength due to the reduction in the signal-to-noise ratio. In the ABE, the $g^{(2)}(0)$ value was greater than 0.5 even at 30 K, and it became larger than 0.6 at 70 K. In contrast, under BBE, the $g^{(2)}(0)$ value became larger than 0.5 above 70 K. It is worth noting that we could achieve $g^{(2)}(0)$ still below 0.5 still at 100 K by applying polarization-controlled QRE to the QD.

3. Conclusion

We proposed a method to improve the optical properties of quantum emitters via polarization-controlled QRE. We applied this QRE to InGaN QDs, which often suffer from the spectral diffusion effect and unwanted background emissions from adjacent emitters. Moreover, accomplishing the high single-photon purity is not easily accessible in InGaN QD due to the fluctuation of indium content in InGaN alloy. In spite of these obstacles, InGaN QDs have advantages in high-temperature operation due to the large exciton binding energy (over thermal energy at room temperature) even under random alloy fluctuation.[46] Furthermore, InGaN QDs can reveal visible light emission, which is valuable for quantum optical applications owing to the high detection efficiency of visible light. Before applying QRE to InGaN QDs embedded in nanowires, μ-PLE spectroscopy was conducted to probe the excited state of the QD. Then, the polarization-dependent absorption measurements were performed under ABE, BBE, and QRE. We measured the unpolarized absorption in the ABE, which was caused

by the absence of polarization selectivity in the GaN barrier. In addition, polarization absorption parallel to the nanowire axis was observed in BBE and was assigned to a crossed transition. However, in QRE, the direction of polarization absorption is perpendicular to the nanowire axis, which is consistent with the polarization direction of the emission. To confirm the effect of polarization-controlled QRE, we compared five excitation conditions (ABE, BBE-pol. max., BBE-pol. min., QRE-pol. max., and QRE-pol. min.). The linewidth with polarization-controlled QRE was 272 μeV, which is much smaller than the 353 μeV for the ABE. In addition, by reducing the background emission near the QD, we observed a second-order correlation value of 0.231 under polarization-controlled QRE, whereas it was 0.47 under ABE. To investigate the possibility of higher-temperature operation, we measured the temperature dependence of the second-order correlation and confirmed that the $g^{(2)}(0)$ value was below 0.5 up to a temperature of 100 K. Therefore, we could selectively pump the excited state of the QD with prohibiting the effect of continuum state absorption.

This research can be applied to other platforms of quantum emitters, such as III-nitride QDs embedded in a pyramid structure, III-As QDs embedded in a pyramid or nanowire structure, and 2D materials. If these systems suffer from spectral diffusion or background emission despite the necessary brightness, polarization-controlled QRE could be the solution. Furthermore, the single-photon purity can be further improved by exploiting other fabrication techniques, such as nanoscale focus pinspot,[31] metallic masking[29,47] of quantum well emission and mesa-etching.[28,48,49] Moreover, we could attempt to curtail the radiative lifetime of QDs for Fourier-transform-limited emission by integrating QDs with dielectric cavities[50,51] or plasmonic cavities[52,53] for future quantum information technologies.

4. Experimental Section

Sample Growth: Self-assembled GaN/InGaN NWs were grown on oxide-free n-type doped Si(111) substrate by molecular beam epitaxy, and active nitrogen was supplied by a radiofrequency plasma cell. Prior to the growth of GaN/InGaN NWs, a 2.5-nm-thick AlN buffer layer was deposited on the substrate following a previously reported procedure,[54] allowing a better control of the NW nucleation, density and orientation.[55–57] The GaN NW bases were grown at 790 °C under N-rich conditions with an N/Ga flux ratio of about 1.36. Then, the substrate temperature was ramped down to 590 °C, under growth interruption to grow QD-shaped InGaN/GaN heterostructures. QD-shaped InGaN was achieved within the In-adlayer growth regime (metal-rich conditions), where a stable Indium layer is adsorbed at the NW growth front, promoting the growth of heterostructures with a disk-like shape.[58] Following this growth procedure, highly homogeneous InGaN QDs with uniform diameters were formed and surrounded by a thin shell of GaN.[58] Finally, a GaN cap layer was grown on top of the heterostructures under N-rich conditions (N/Ga ratio of 25) at 650 °C to preserve abrupt InGaN/GaN interfaces.

Optical Experiment: A tunable femtosecond Ti:sapphire pulsed laser (pulse duration = 200 fs; repetition rate = 80 MHz) was used as the excitation laser. Low vibration closed-loop liquid-helium cryostation was used to measure a single QD under low-temperature conditions. The laser was focused on a single QD, and the emission of an identical QD was collected using a microscope objective lens (Mitutoyo; 50×; N.A., 0.65). PL spectra were analyzed using a high-resolution monochromator (Princeton Instruments, SP2750). To measure the second-order photon correlation, the Hanbury–Brown and Twiss experimental setup with a 50:50 beam splitter and two avalanche photodiodes (APDs) (ID Quantique; ID 100; temporal resolution, 40 ps) were utilized. In addition, two avalanche photodiodes were connected to a time-correlated single-photon counting system (Picoquant; Picoharp 300) to obtain coincidence histograms as a function of delay times between two detected photons at the APDs. In the second-order correlation measurements, spectral filtering with the bandwidth of about 0.7 nm was used.

Supporting Information

Supporting Information is available from the Wiley Online Library or from the author.

Acknowledgements

This work was supported by the National Research Foundation (2020M3E4A1080112, 2022R1A2B5B03002560), Institute of Information & Communications Technology Planning & Evaluation (IITP) grant (No. 2020-0-00841) funded by the Korea government, Samsung Science and Technology Foundation under Project No. SSTF-BA1602-05, French National Research Agency through the Project SCENIC (ANR-20-CE09-0005), and by the French Renatech/Renatch + networks.

Conflict of Interest

The authors declare no conflict of interest.

Author Contributions

Y.-H.C. supervised the project. S.J. designed and performed experiments. M.C. prepared the dispersed nanowire samples and performed the SEM and TEM measurements. B.K. supported the optical analysis. M.M., M.T., and N.G. grew the nanowire samples. H.G.S. and H.S.Y. supported the analysis. S.J. and Y.-H.C. wrote the manuscript. All the authors discussed the results and commented on the manuscript.

Data Availability Statement

The data that support the findings of this study are available from the corresponding author upon reasonable request.

Keywords

linewidth, nanowires, polarization, quantum dots, quantum emitters, quasi-resonant excitation, single-photon purity

Received: August 25, 2022
Revised: November 18, 2022
Published online: November 30, 2022

[1] V. Giovannetti, S. Lloyd, L. Maccone, *Science* **2004**, *306*, 1330.
[2] S. Slussarenko, M. M. Weston, H. M. Chrzanowski, L. K. Shalm, V. B. Verma, S. W. Nam, G. J. Pryde, *Nat. Photonics* **2017**, *11*, 700.
[3] J. L. O'Brien, *Science* **2007**, *318*, 1567.
[4] E. Knill, R. Laflamme, G. J. Milburn, *Nature* **2001**, *409*, 46.

[5] M. K. Bhaskar, R. Riedinger, B. Machielse, D. S. Levonian, C. T. Nguyen, E. N. Knall, H. Park, D. Englund, M. Loncar, D. D. Sukachev, M. D. Lukin, *Nature* **2020**, *580*, 60.
[6] A. Beveratos, R. Brouri, T. Gacoin, A. Villing, J. P. Poizat, P. Grangier, *Phys. Rev. Lett.* **2002**, *89*, 187901.
[7] B. Darquie, M. P. A. Jones, J. Dingjan, J. Beugnon, S. Bergamini, Y. Sortais, G. Messin, A. Browaeys, P. Grangier, *Science* **2005**, *309*, 454.
[8] M. Koperski, K. Nogajewski, A. Arora, V. Cherkez, P. Mallet, J. Y. Veuillen, J. Marcus, P. Kossacki, M. Potemski, *Nat. Nanotechnol.* **2015**, *10*, 503.
[9] T. M. Babinec, B. J. Hausmann, M. Khan, Y. Zhang, J. R. Maze, P. R. Hemmer, M. Loncar, *Nat. Nanotechnol.* **2010**, *5*, 195.
[10] X. He, N. F. Hartmann, X. Ma, Y. Kim, R. Ihly, J. L. Blackburn, W. Gao, J. Kono, Y. Yomogida, A. Hirano, T. Tanaka, H. Kataura, H. Htoon, S. K. Doorn, *Nat. Photonics* **2017**, *11*, 577.
[11] T. T. Tran, K. Bray, M. J. Ford, M. Toth, I. Aharonovich, *Nat. Nanotechnol.* **2016**, *11*, 37.
[12] H. Utzat, W. Sun, A. E. K. Kaplan, F. Krieg, M. Ginterseder, B. Spokoyny, N. D. Klein, K. E. Shulenberger, C. F. Perkinson, M. V. Kovalenko, M. G. Bawendi, *Science* **2019**, *363*, 1068.
[13] Q. Jiang, P. Roy, J. B. Claude, J. Wenger, *Nano Lett.* **2021**, *21*, 7030.
[14] I. Aharonovich, D. Englund, M. Toth, *Nat. Photonics* **2016**, *10*, 631.
[15] A. W. Elshaari, W. Pernice, K. Srinivasan, O. Benson, V. Zwiller, *Nat. Photonics* **2020**, *14*, 285.
[16] M. Choi, S. Kim, S. Choi, Y.-H. Cho, *Appl. Phys. Lett.* **2021**, *119*, 134001.
[17] S. E. Thomas, M. Billard, N. Coste, S. C. Wein, H. P. Ollivier, O. Krebs, L. Tazairt, A. Harouri, A. Lemaitre, I. Sagnes, C. Anton, L. Lanco, N. Somaschi, J. C. Loredo, P. Senellart, *Phys. Rev. Lett.* **2021**, *126*, 233601.
[18] T. Müller, J. Skiba-Szymanska, A. B. Krysa, J. Huwer, M. Felle, M. Anderson, R. M. Stevenson, J. Heffernan, D. A. Ritchie, A. J. Shields, *Nat. Commun.* **2018**, *9*, 862.
[19] S. Deshpande, J. Heo, A. Das, P. Bhattacharya, *Nat. Commun.* **2013**, *4*, 1675.
[20] J. Zhang, J. S. Wildmann, F. Ding, R. Trotta, Y. Huo, E. Zallo, D. Huber, A. Rastelli, O. G. Schmidt, *Nat. Commun.* **2015**, *6*, 10067.
[21] T. Jemsson, H. Machhadani, K. F. Karlsson, C.-W. Hsu, P.-O. Holtz, *Appl. Phys. Lett.* **2014**, *105*, 081901.
[22] M. J. Holmes, K. Choi, S. Kako, M. Arita, Y. Arakawa, *Nano Lett.* **2014**, *14*, 982.
[23] J. H. Kim, Y. H. Ko, S. H. Gong, S. M. Ko, Y. H. Cho, *Sci. Rep.* **2013**, *3*, 2150.
[24] M. Holmes, S. Kako, K. Choi, M. Arita, Y. Arakawa, *Phys. Rev. B* **2015**, *92*, 115447.
[25] G. Sallen, A. Tribu, T. Aichele, R. André, L. Besombes, C. Bougerol, M. Richard, S. Tatarenko, K. Kheng, J. P. Poizat, *Nat. Photonics* **2010**, *4*, 696.
[26] L. Tao, W. Wei, Y. Li, W. Ou, T. Wang, C. Wang, J. Zhang, J. Zhang, F. Gan, X. Ou, *ACS Photonics* **2020**, *7*, 2723.
[27] P. Schnauber, J. Schall, S. Bounouar, T. Hohne, S. I. Park, G. H. Ryu, T. Heindel, S. Burger, J. D. Song, S. Rodt, S. Reitzenstein, *Nano Lett.* **2018**, *18*, 2336.
[28] M. Gschrey, F. Gericke, A. Schüßler, R. Schmidt, J. H. Schulze, T. Heindel, S. Rodt, A. Strittmatter, S. Reitzenstein, *Appl. Phys. Lett.* **2013**, *102*, 251113.
[29] T. Jemsson, H. Machhadani, P. O. Holtz, K. F. Karlsson, *Nanotechnology* **2015**, *26*, 065702.
[30] S.-H. Gong, S. Kim, J.-H. Kim, J.-H. Cho, Y.-H. Cho, *ACS Photonics* **2018**, *5*, 711.
[31] M. Choi, S. Jun, K. Y. Woo, H. G. Song, H. S. Yeo, S. Choi, D. Park, C. H. Park, Y. H. Cho, *ACS Nano* **2021**, *15*, 11317.
[32] M. N. Makhonin, J. E. Dixon, R. J. Coles, B. Royall, I. J. Luxmoore, E. Clarke, M. Hugues, M. S. Skolnick, A. M. Fox, *Nano Lett.* **2014**, *14*, 6997.
[33] G. Reithmaier, M. Kaniber, F. Flassig, S. Lichtmannecker, K. Muller, A. Andrejew, J. Vuckovic, R. Gross, J. J. Finley, *Nano Lett.* **2015**, *15*, 5208.
[34] T. Huber, M. Davanco, M. Müller, Y. Shuai, O. Gazzano, G. S. Solomon, *Optica* **2020**, *7*, 380.
[35] E. B. Flagg, A. Muller, J. W. Robertson, S. Founta, D. G. Deppe, M. Xiao, W. Ma, G. J. Salamo, C. K. Shih, *Nat. Phys.* **2009**, *5*, 203.
[36] H. S. Nguyen, G. Sallen, C. Voisin, P. Roussignol, C. Diederichs, G. Cassabois, *Phys. Rev. Lett.* **2012**, *108*, 057401.
[37] G. Wrigge, I. Gerhardt, J. Hwang, G. Zumofen, V. Sandoghdar, *Nat. Phys.* **2007**, *4*, 60.
[38] C. Matthiesen, A. N. Vamivakas, M. Atature, *Phys. Rev. Lett.* **2012**, *108*, 093602.
[39] M. Holmes, S. Kako, K. Choi, P. Podemski, M. Arita, Y. Arakawa, *Phys. Rev. Lett.* **2013**, *111*, 057401.
[40] B. P. L. Reid, C. Kocher, T. Zhu, F. Oehler, R. Emery, C. C. S. Chan, R. A. Oliver, R. A. Taylor, *Appl. Phys. Lett.* **2014**, *104*, 263108.
[41] K. Sebald, H. Lohmeyer, J. Gutowski, T. Yamaguchi, D. Hommel, *Phys. Status Solidi C* **2006**, *3*, 3864.
[42] A. Vasanelli, R. Ferreira, G. Bastard, *Phys. Rev. Lett.* **2002**, *89*, 216804.
[43] J.-H. Kim, T. Cai, C. J. K. Richardson, R. P. Leavitt, E. Waks, *Optica* **2016**, *3*, 577.
[44] R. Anufriev, J. B. Barakat, G. Patriarche, X. Letartre, C. Bru-Chevallier, J. C. Harmand, M. Gendry, N. Chauvin, *Nanotechnology* **2015**, *26*, 395701.
[45] G. Visimberga, G. Rainò, A. Salhi, V. Tasco, M. T. Todaro, L. Martiradonna, M. De Giorgi, A. Passaseo, R. Cingolani, M. De Vittorio, *Appl. Phys. Lett.* **2008**, *93*, 151112.
[46] S. K. Patra, S. Schulz, *Nano Lett.* **2020**, *20*, 234.
[47] T. Yamamoto, M. Maekawa, Y. Imanishi, S. Ishizawa, T. Nakaoka, K. Kishino, *Jpn. J. Appl. Phys.* **2016**, *55*, 04ek03.
[48] H. P. Springbett, J. Jarman, T. Zhu, M. Holmes, Y. Arakawa, R. A. Oliver, *Appl. Phys. Lett.* **2018**, *113*, 101107.
[49] B.-Y. Wang, T. Häyrynen, L. Vannucci, M. A. Jacobsen, C.-Y. Lu, N. Gregersen, *Appl. Phys. Lett.* **2021**, *118*, 114003.
[50] F. Liu, A. J. Brash, J. O'Hara, L. Martins, C. L. Phillips, R. J. Coles, B. Royall, E. Clarke, C. Bentham, N. Prtljaga, I. E. Itskevich, L. R. Wilson, M. S. Skolnick, A. M. Fox, *Nat. Nanotechnol.* **2018**, *13*, 835.
[51] X. Ding, Y. He, Z. C. Duan, N. Gregersen, M. C. Chen, S. Unsleber, S. Maier, C. Schneider, M. Kamp, S. Hofling, C. Y. Lu, J. W. Pan, *Phys. Rev. Lett.* **2016**, *116*, 020401.
[52] B. Demory, A. Katcher, T. Hill, C.-H. Teng, C. Zhang, L. J. Guo, H. Deng, P. C. Ku, *ACS Photonics* **2017**, *4*, 795.
[53] S. H. Gong, J. H. Kim, Y. H. Ko, C. Rodriguez, J. Shin, Y. H. Lee, S. Dangle , X. Zhang, Y. H. Cho, *Proc. Natl. Acad. Sci. USA* **2015**, *112*, 5280.
[54] L. Largeau, E. Galopin, N. Gogneau, L. Travers, F. Glas, J.-C. Harmand, *Cryst. Growth Des.* **2012**, *12*, 2724.
[55] M. D. Brubaker, I. Levin, A. V. Davydov, D. M. Rourke, N. A. Sanford, V. M. Bright, K. A. Bertness, *J. Appl. Phys.* **2011**, *110*, 053506.
[56] R. Songmuang, O. Landré, B. Daudin, *Appl. Phys. Lett.* **2007**, *91*, 251902.
[57] K. A. Bertness, A. Roshko, L. M. Mansfield, T. E. Harvey, N. A. Sanford, *J. Cryst. Growth* **2007**, *300*, 94.
[58] M. Morassi, L. Largeau, F. Oehler, H.-G. Song, L. Travers, F. H. Julien, J.-C. Harmand, Y.-H. Cho, F. Glas, M. Tchernycheva, N. Gogneau, *Cryst. Growth Des.* **2018**, *18*, 2545.